INDEPTH III seismic data: From surface observations to deep crustal processes in Tibet

Seth S. Haines,[1] Simon L. Klemperer,[1] Larry Brown,[2] Guo Jingru,[2] James Mechie,[3] Rolf Meissner,[4] Andrew Ross,[5] and Zhao Wenjin[6]

Received 13 June 2001; revised 22 July 2002; accepted 1 August 2002; published 22 January 2003.

[1] During the summer of 1998, active-source seismic data were collected along a transect running 400 km NNW-SSE across the central Tibetan Plateau as the third phase of project INDEPTH (International Deep Profiling of Tibet and the Himalaya). The transect extends northward from the central Lhasa block, across the Jurassic Bangong-Nujiang Suture (BNS) at 89.5°E, to the central Qiangtang block. A seismic velocity model for the transect to ~25 km depth produced by inversion of *P* wave first arrivals on ~3000 traces shows (1) a ~50-km-wide region of low velocity (at least 5% less than surrounding velocities) extending to the base of the model at the BNS; (2) sedimentary cover for the southern Qiangtang block that is ~3.5 km thick; (3) a distinct interface between sedimentary cover and Qiangtang basement or underplated Jurassic melange in the central Qiangtang block; and (4) evidence that the Bangoin granite extends to a depth of at least 15 km. The BNS has little geophysical signature, and appears unrelated to the ~5 km northward shallowing of the Moho which is associated with the BNS in central Tibet. Geophysical data along the main INDEPTH III transect show little evidence for widespread crustal fluids, in contrast to the seismic ''bright spots'' found in southern Tibet and to magnetotelluric evidence of fluid accumulations in eastern Tibet. A comparison between the global average and Tibetan velocity-depth functions offers constraints for models of plateau uplift and crustal thickening. Taken together with the weak geophysical signature of the BNS, these velocity-depth functions suggest that convergence has been accommodated largely through pure-shear thickening accompanied by removal of lower crustal material by lateral escape, likely via ductile flow. Although we cannot resolve the details, we believe lateral lower crustal flow has overprinted or destroyed evidence in the deep crust for the earlier assembly of Tibet as a series of accreted terranes. *INDEX TERMS:* 8110 Tectonophysics: Continental tectonics—general (0905); 8120 Tectonophysics: Dynamics of lithosphere and mantle—general; 9320 Information Related to Geographic Region: Asia; 0905 Exploration Geophysics: Continental structures (8109, 8110); *KEYWORDS:* Tibet, INDEPTH, seismic, tectonics, plateau. **Citation:** Haines, S. S., S. L. Klemperer, L. Brown, G. Jingru, J. Mechie, R. Meissner, A. Ross, and Z. Wenjin, INDEPTH III seismic data: From surface observations to deep crustal processes in Tibet, *Tectonics*, *22*(1), 1001, doi:10.1029/2001TC001305, 2003.

1. Introduction and Geologic Setting

[2] The Tibetan Plateau is a unique feature on the Earth's surface, but from the processes occurring there we can draw inferences regarding the evolution of other continent-continent collision zones. Despite its value as a natural laboratory for studies of collisional tectonics (and partly due to the inaccessibility of its imposing topography), many basic questions still persist in our understanding of the plateau. Most fundamentally, a thorough understanding of the mechanism(s) responsible for regional uplift and accommodation of shortening remains elusive. Our new geophysical data, collected as part of the third phase of Project INDEPTH III (International Deep Profiling of Tibet and the Himalayas), provide constraints on large-scale tectonic models, and on smaller-scale geologic questions.

[3] Between the Tethyan Himalaya in the far south and the Songpan-Ganzi terrane in the far north, the Tibetan Plateau is made up of two main crustal blocks: the Lhasa block south of the Qiangtang block (Figures 1 and 2). This ''traditional'' description of Tibet in terms of multiple terranes sequentially accreted to Asia obscures, as we discuss later, the fundamental processes governing Tertiary uplift and shortening. Between the Lhasa and Qiangtang blocks lies a dismembered ophiolite sequence and related melange complex; both are semi-continuous in an east-west zone across Tibet and define what is commonly referred to as the Bangong-Nujiang Suture (BNS) (Figure 1). Geochemically similar Jurassic ophiolitic fragments with calc-alkaline volcanic rocks and high-magnesium dolerite dikes were scattered over the northern 150 km of the Lhasa block during the Late Jurassic to Early Cretaceous [*Chang et al.*, 1986; *Coward et al.*, 1988; *Girardeau et al.*, 1984, 1985,

[1]Department of Geophysics, Stanford University, Stanford, California, USA.
[2]Department of Geological Sciences, Cornell University, Ithaca, New York, USA.
[3]GeoForschungsZentrum Potsdam (GFZ), Potsdam, Germany.
[4]Institute of Geoscience, Kiel University, Kiel, Germany.
[5]Geological Institute, University of Copenhagen, Denmark.
[6]Chinese Academy of Geological Sciences, Beijing, China.

0278-7407/03/2001TC001305$12.00

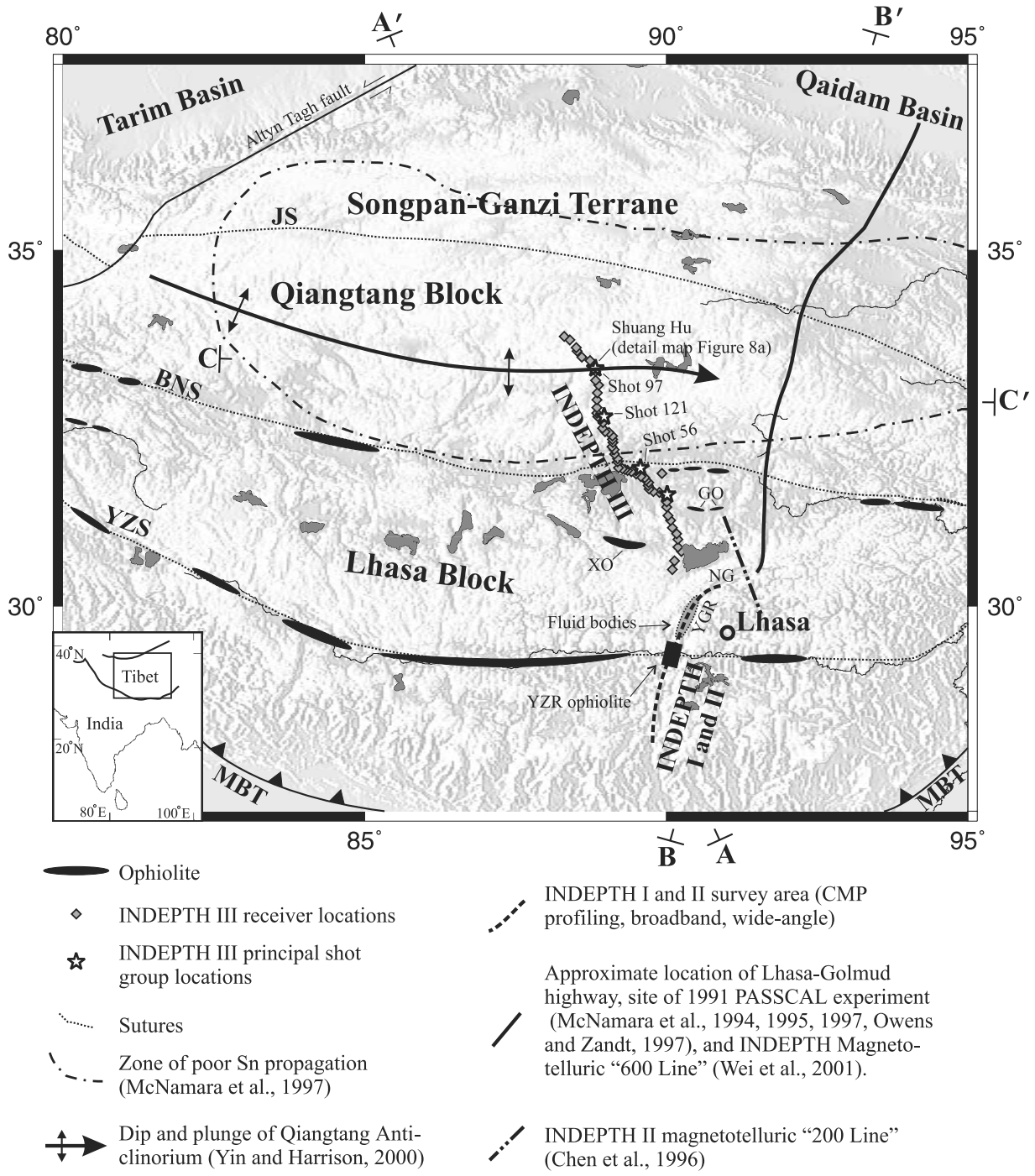

Figure 1. Shaded relief map of Tibet, showing INDEPTH III seismic and magnetotelluric transects, locations of shots 56, 121, and 97 (data in Figure 5), and locations of ophiolite associated with the Bangong-Nujiang Suture (BNS) and Yarlung-Zangbo Suture (YZS) [after *Kidd et al.*, 1988; *Liu et al.*, 1986; *Zhao et al.*, 1984]. Also shown are locations of cross sections A-A′, B-B′ and C-C′ (Figure 9), Jinsha Suture (JS), Main Boundary Thrust (MBT), location of Yarlung Zangbo Reflector (YZR) ophiolite [*Makovsky et al.*, 1999], Yadong-Gulu Rift (YGR), Nyainqentanglha Graben (NG), locations of Xianxa (XO) and Gyanco/Donqiao ophiolites (GO).

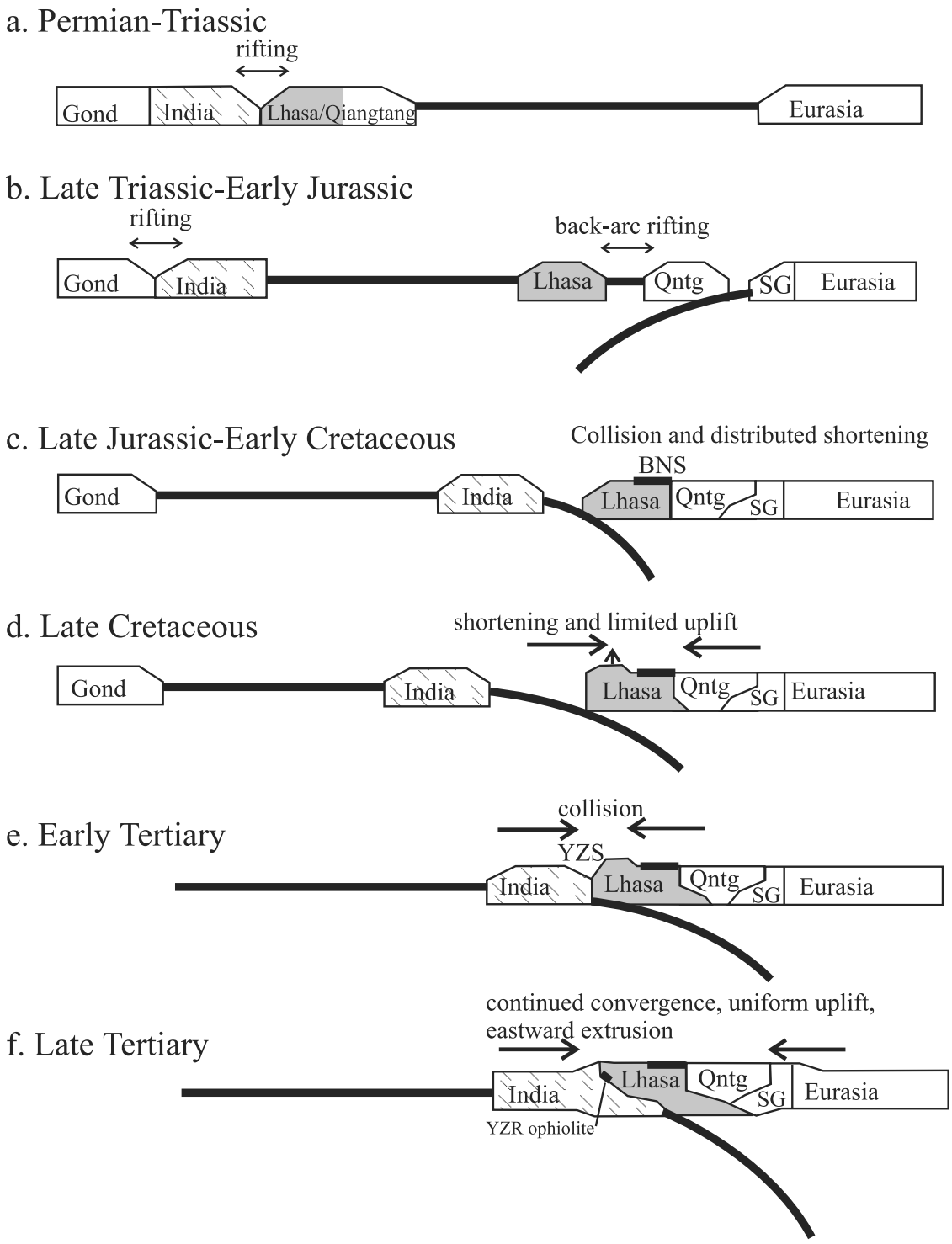

Figure 2. Evolution of Tibetan Plateau, cartoon time series modified after *Yin and Harrison* [2000] and *Allegre et al.* [1984]. We suggest that Lhasa and Qiangtang blocks originate as a single terrane (a), and undergo back arc rifting in the Late Triassic (b), leading to the creation of a small ocean which closes in the Late Jurassic/Early Cretaceous (c). ''YZR ophiolite'' in (f) is ophiolitic material imaged near Yarlung Zangbo Suture (YZS) by *Makovsky et al.* [1999]. Abbreviations: Bangong-Nujiang Suture (BNS), Songpan-Ganzi Terrane (SG), Gondwana (Gond), Qiangtang block (Qntg).

1986]. Extending north from the ophiolite belt lies a broad (tens of kilometers) band of flysch deposits. North dipping subduction near the northern margin of the ophiolite belt, accompanied by southward thrusting of an ophiolitic nappe, now exposed as multiple klippen, over the northern Lhasa block has been inferred by past authors [e.g. *Coward et al.*, 1988], but may not be required by the assembled data.

[4] A ~5 km northward step-up of the Moho located near the BNS has been reported by *Zhao et al.* [2001], in agreement with similar results from previous authors [*Owens and Zandt*, 1997], but refuting the ~20 km Moho offset proposed by *Hirn et al.* [1984]. Teleseismic results [e.g. *Huang et al.*, 2000; *McNamara et al.*, 1997] indicate a pronounced N-S change in lower crustal and upper mantle seismic properties located below the approximate surface trace of the BNS. We suggest that these features and the suture are unrelated, and that there is little or no evidence for the BNS continuing through the lower crust at the present.

[5] Seismic reflection and magnetotelluric profiling in southern Tibet have revealed the presence of fluid concentrations at 15 km depth [*Brown et al.*, 1996; *Chen et al.*, 1996], probably constituting transient accumulations of pneumatolytic brines above cooling intrusions [*Makovsky and Klemperer*, 1999]. These concentrations extend for a N-S distance of at least 100 km, along the Yadong-Gulu Rift from north of the Yarlung Zangbo Suture to the Nyainqentanglha Graben (Figure 1). The E-W extent of these concentrations cannot be constrained by the existing 2-D seismic data, though the resolution of highly conductive material in the magnetotelluric "200 Line" (Figure 1) [*Chen et al.*, 1996] suggests that fluid concentrations extend east beyond the rift zone and north to at least 31°N. The shallow Curie isotherm suggested by the pronounced satellite magnetic low associated with the entire Tibetan Plateau [*Alsdorf and Nelson*, 1999], active volcanism widespread across the Qiangtang block, and magnetotelluric results [*Wei et al.*, 2001] all support the hypothesis that melt also exists at least locally within the crust of central and northern Tibet. However, the identification of anhydrous lower crustal xenoliths [*Hacker et al.*, 2000] suggests a dearth of aqueous fluids and anatectic melt in the crust of northern Tibet. Furthermore, earthquake surface-wave analysis shows that no low-velocity zone exists within the crust of northern Tibet [*Rapine et al.*, 2002] suggesting that crustal fluids are rare in northern Tibet. Thus it is unclear whether widespread fluid accumulations exist within Tibetan crust north of 31°N; we suggest (below) that the data can best be satisfied by W-E as well as N-S variation in crustal conditions and properties.

[6] We then explain the aforementioned results—lack of evidence for the BNS in the lower crust and regional variations in crustal fluid content—with a model for processes now active in the Tibetan Plateau. A number of different hypotheses have been proposed to explain the development and deformation of the Tibetan Plateau (Figure 3). Models range from crustal doubling by wholesale underplating of Indian crust beneath Asia [e.g. *Powell and Conaghan*, 1973], to pure-shear thickening of Asian crust by India acting as a rigid indenter [e.g., *Houseman and England*, 1996]. Most physically plausible models fall between these two end-members, calling for partial injection of Indian crust into Asian lithosphere, either through rigid crustal underplating [e.g., *Barazangi and Ni*, 1982], perhaps accompanied by thrusting of Lhasa block lower crust beneath the Qiangtang block [*Yin and Harrison*, 2000]; or through hydraulic (ductile) thickening of Asian lower crust [e.g., *Zhao and Morgan*, 1987; *Kola-Ojo and Meissner*, 2001]. Models for accommodation of convergence (Figure 3) range from ductile flow of the lower crust [e.g., *Clark and Royden*, 2000] and/or upper mantle [*Owens and Zandt*, 1997; *Huang et al.*, 2000] to large-scale block motion along strike-slip faults [e.g., *Molnar and Tapponnier*, 1975] to eclogitization of lower crustal material [e.g., *Sapin and Hirn*, 1997]. In principle, these different models predict different velocity-depth profiles through the crust (Figure 3, right-hand column). Hence, our INDEPTH III seismic velocity models provide new constraints for these models and their relation to large-scale structures of the Tibetan Plateau.

2. Data Acquisition and Processing

2.1. INDEPTH III Seismic Data

[7] Project INDEPTH was initiated in the early 1990s as a multi-disciplinary international collaboration with the goal of constraining the mechanisms responsible for the accommodation of India-Asia convergence and the uplift of the Tibetan Plateau. INDEPTH III included passive [*Huang et al.*, 2000; *Rapine et al.*, 2002] and active source [*Zhao et al.*, 1999, 2001] seismic surveys on multiple scales, as well as magnetotelluric [*Wei et al.*, 2001; *Solon et al.*, 2000] and geologic [*Hacker et al.*, 2000; *Blisniuk et al.*, 2001] studies.

Figure 3. (opposite) Block diagrams of uplift models for Tibetan Plateau and velocity-depth function expected for each (bold line), plotted with Tibet velocities from the Lhasa (thin dashed line) and Qiangtang (thin solid line) blocks [from *Zhao et al.*, 2001]. Predicted velocity function (bold line) is global average of *Christensen and Mooney* [1995] (in a), modified in b through f by thinning or thickening, without correction for pressure, temperature or metamorphism. a) "average" 42-km-thick crust (global weighted average crust of *Christensen and Mooney* [1995]); b) convergence accommodated by wholesale underthrusting [e.g., *Powell and Conaghan*, 1973]. In this case, the starting crust is 32.5 km thick in order to result in Tibetan 65-km-thick crust; c) "hydraulic thickening" of Asian lower crust in response to injection of rigid Indian lower crust [e.g., *Zhao and Morgan*, 1987]; d) pure shear thickening of Asian crust [e.g., *Houseman and England*, 1996]; e) pure-shear thickening of Asian crust, accompanied by removal of lower and middle crust by lateral ductile flow [e.g., *Clark and Royden*, 2000]; f) pure shear thickening of Asian crust, accompanied by removal of middle crust by lateral ductile flow; g) pure shear thickening of Asian crust accompanied by removal of lower crust by conversion to eclogite [e.g., *Sapin and Hirn*, 1997].

a. Starting condition: “average” 42-km thick crust.

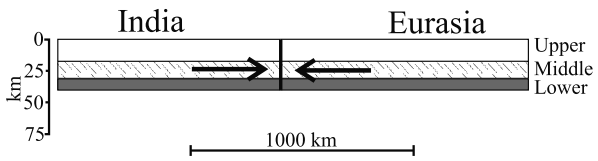

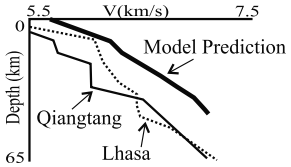

b. Wholesale underthrusting (1000 km convergence)

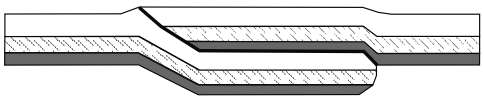

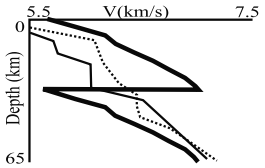

c. Injection and hydraulic thickening of lower crust (600 km convergence)

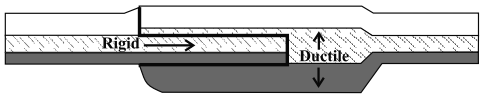

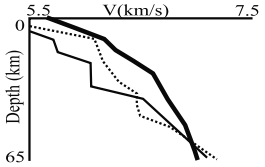

d. Pure shear thickening (500 km convergence)

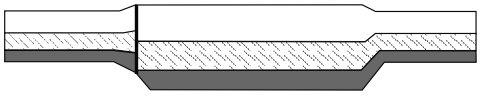

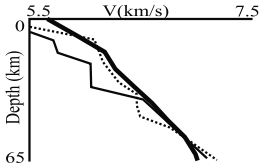

e. Pure-shear thickening with middle and lower crustal ductile flow (1000 km convergence)

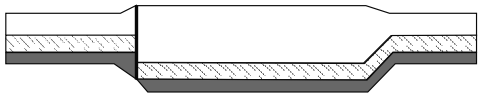

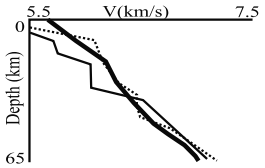

f. Pure-shear thickening with middle crustal ductile flow (~700 km convergence)

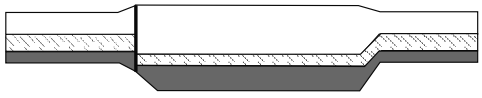

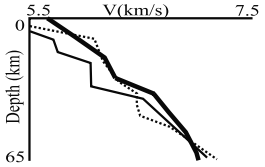

g. Pure-shear thickening with conversion of lower-crustal material to eclogite (below the Moho) (~800 km convergence)

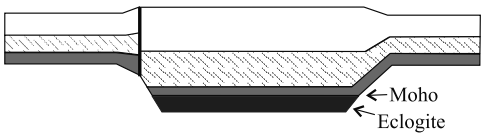

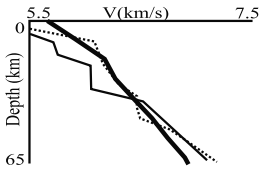

Here we discuss the seismic reflection and refraction data collected along a 400-km transect running NNW-SSE across the BNS at about 89.5°E (see Figure 1).

[8] We deployed 51 broadband (mainly Streckeisen STS-2) and intermediate-period seismometers at 5 to 10 km intervals along the main INDEPTH transect (Figure 1), and 8 instruments in a perpendicular transect along the BNS (not shown). To gain higher resolution of crustal structure we augmented this coarse array with a dense array of fifteen closely spaced (1 to 2 km) RefTek seismographs equipped with Mark Products 4.5 Hz 3-component L-28 geophones, and with a 60 channel, 2-km, Geometrics system with 4.5 Hz vertical geophones, all deployed successively at four groups of dynamite shots (see Figure 1). Approximately 160 small (2 to 50 kg) shots were grouped at four key locations along the transect, in addition to the 11 large shots (180 to 1160 kg) that were distributed along the transect. The coarse 51-instrument array was then reconfigured and left to record earthquakes for one year. All seismic data are available for download at www.iris.edu.

[9] Processing of the wide-angle data from the 11 large shots has been accomplished by J. Mechie at GeoForschungsZentrum Potsdam (GFZ), and the resulting crustal velocity model is presented by *Zhao et al.* [2001] and is shown here in Figure 4c. *Zhao et al.* [1999] present the reflection sections resulting from processing of the data collected by the Geometrics unit. In this contribution we present an analysis of data from all shots as collected by the entire array, excluding the Geometrics (30-m spaced receivers), principally a velocity model for the upper 25 km of the crust which provides detail beyond the *Zhao et al.* [2001] model.

2.2. Refraction Modeling

[10] We used ~3000 first-break picks from the RefTek data to construct an upper crustal (to a subsurface depth of 25 km) velocity model for the INDEPTH III seismic transect. The model (shown in Figure 4b) consists of three layers: (1) a thin (0.5 to 1 km) upper layer that represents the Neogene sedimentary cover and weathered layer, (2) a ~4-km-thick layer that broadly represents the Phanerozoic sedimentary units, and (3) a ~15-km-thick layer representing basement units. Velocities for the uppermost layer were determined through forward modeling using ray-tracing techniques described by *Zelt and Smith* [1992], and by selecting uppermost velocities appropriate to the rock types present at the surface [*Kidd et al.*, 1988; *Liu et al.*, 1986; *Zhao et al.*, 1984]. Velocities for the middle and lower layer were determined first through downward extrapolation of the velocities of layer 1, and then through forward modeling followed by damped least squares inverse modeling using the computer code RayInvr [see *Zelt and Smith*, 1992]. The positions of the layer boundaries were determined through forward modeling, with some adjustments made by inversion modeling simultaneous with velocity inversion.

[11] The model is defined by 67 independent velocity nodes and 30 boundary nodes. Node spacing is closest in the upper two layers (20 to 50 km, or less where forward modeling requires spatially rapid velocity changes), and coarser in the deeper layers (up to 150 km at the bottom of the model). Because layer 1 and layer 2 velocities were determined through forward modeling (with some inverse modeling, in the case of layer 2), node resolution is not a meaningful gauge of model reliability. The diagonal elements of the resolution matrix for velocity nodes along the upper boundary of layer 3 have an average value of 0.63, while diagonal elements of the resolution matrix corresponding with nodes along the lower boundary of that layer average 0.18 [see, e.g., *Zelt and Smith*, 1992]. Nodes that specify layer boundary positions are generally poorly resolved due to the minimal velocity contrast across layer boundaries. The model fits 2932 travel time picks with a root mean squared (RMS) travel time residual of 0.20 s. We believe model misfit is largely a result of non-linearity of the seismic transect (this is a two-dimensional model developed from three-dimensional data).

[12] Important features of the model (Figure 4b) include (1) a ~50-km-wide region of low velocity (at least 5% less than surrounding velocities) extending vertically to the base of the model below the surface trace of the BNS (shown by low apparent velocity of arrivals to the north of shot 56 and to the south of shot 97, Figures 5a and 5c); (2) a body ~3.5 km thick with a velocity of 4 to 5 km/s interpreted as the fault-thickened Phanerozoic flysch deposits on the southern Qiangtang block (note low apparent velocity of first arrivals at receivers to the south of shots 121 and 97, Figures 5b and 5c); (3) a distinct interface between the layer interpreted as sedimentary cover (velocity 4 to 5 km/s) and a deeper layer with velocity 5.8 to 6 km/s (likely Jurassic melange or Qiangtang basement) at ~3 km depth in the vicinity of Shuang Hu (see data in Figures 5b and 5c, note high apparent velocity of first arrivals at receivers to the north of shots 121 and 97); and (4) a relatively high-velocity body (~6.0 km/s) extending to a depth of at least 15 km (where it becomes indistinguishable from surrounding velocities) below the surface exposure of the Bangoin granite, suggesting that the pluton extends to at least this depth (evidenced by high apparent velocity of arrivals to the south of shot 56, Figure 5a).

[13] The model presented here incorporates a larger number of shots with finer shot spacing so provides greater resolution than the model of *Zhao et al.* [2001] (Figure 4c), and permits the interpretation of finer features. Our model fits well with the corresponding (upper 25 km) part of the crustal-scale model presented by *Zhao et al.* [2001], which has resolution limited by the smaller number of shots incorporated. Agreement is good for the important trends, particularly the region of low velocity at the BNS and the generally slower velocities for the Qiangtang block relative to the Lhasa block.

2.3. Reflection Profiling

[14] In addition to velocity modeling, we also attempted to create single-fold near-vertical reflection sections. However, despite extensive processing of our INDEPTH III data, we were unable to image coherent reflectivity. Individual shot and receiver gathers show few, if any, distinct phases after the first arrivals. Single-fold midpoint sections were

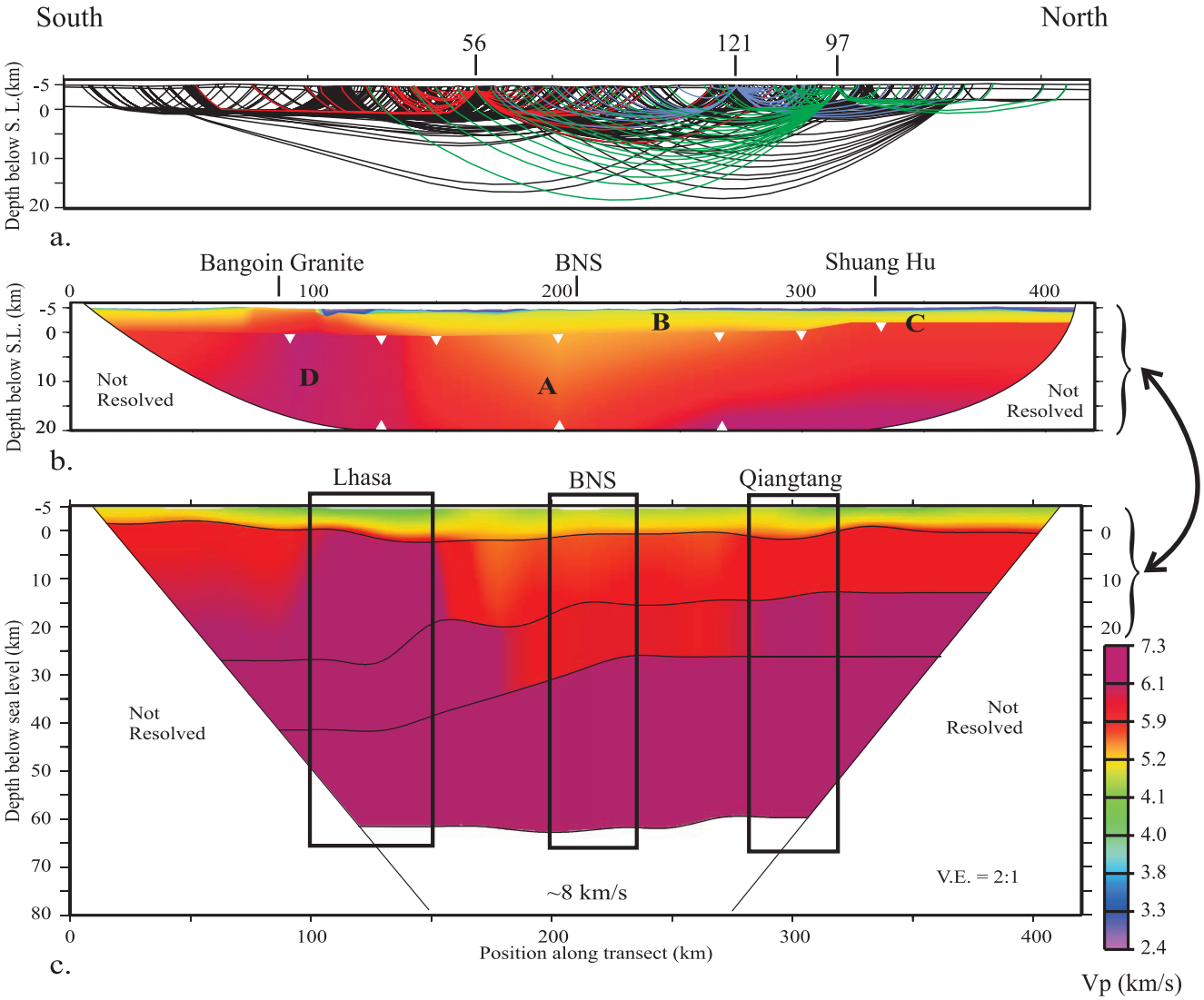

Figure 4. Seismic *P* wave velocity models with vertical exaggeration = 2:1. a) Diagram of ray coverage for model presented in this paper (shown in b). Red, blue, and green rays were recorded from shots 56, 121, and 97 (Figure 5). Thin black lines show layer boundaries. b) Velocity model developed from ~3000 first break picks from all (~170) INDEPTH III dynamite shots. Bold letters refer to features mentioned in text: A: Region of low velocity at Bangong-Nujiang Suture (BNS), B: ~3.5 km of Phanerozoic sediment in the southern Qiangtang block, C: distinct interface between sedimentary units and higher velocity (melange?) material, D: evidence of extent of Bangoin granite to depth. White triangles show locations of velocity nodes for the third (lowest) layer. Nodes in other layers are too numerous to show. c) Velocity model from *Zhao et al.* [2001] developed from 11 "large" shots. Black boxes outline swaths averaged for velocity functions used for comparison with uplift models (shown in Figures 3 and 10).

constructed using traces with maximum offsets between 30 and 60 km, with normal moveout correction velocities derived from our and *Zhao et al.* [2001] velocity models. True-amplitude, automatic-gain-controlled, and energy sections (squared amplitudes) were examined using band-pass filters ranging from about 2 to 30 Hz.

[15] Processing of the Geometrics data (30 m receiver spacing) shows coherent reflectivity from 10 to 22 seconds two-way travel time (TWTT) at the base of the crust [*Zhao et al.*, 1999; A. Ross, personal communication, 2000]. That this reflectivity does not appear on RefTek data (~2 km receiver spacing) profiles is not necessarily contradictory, however. The Geometrics data midpoints are at approximately 16 m intervals, and sections are the result of up to fivefold stacking. RefTek data have, at best, 125 m midpoint spacing and lack redundancy needed for stacking. The reflectivity observed in the Geometrics sections is of relatively low amplitude and individual reflections are not

laterally continuous for more than ~2 km. Thus it is likely that RefTek data coverage is simply too sparse to resolve lower crustal reflectivity.

3. Interpretation

3.1. Bangong-Nujiang Suture (BNS)

[16] Two important but unresolved questions about the BNS are how was it formed, and how is it related to the Moho step and change in mantle properties with which it is spatially associated [*Kosarev et al.*, 1999]. The BNS is defined by a 150-km-wide belt of scattered Jurassic ophiolite and related melange material that was emplaced on the northern Lhasa block during the latest Jurassic or earliest Cretaceous [*Girardeau et al.*, 1986]. The northern half of the Lhasa block was shortened as much as 60% during and after the emplacement of the ophiolite material [*Murphy et al.*, 1997]. The rock types on either side of the BNS (the Lhasa and Qiangtang blocks) are not strikingly different (mainly Mesozoic shallow marine sedimentary units) [*Kidd et al.*, 1988].

[17] INDEPTH III provides some of the first geophysical data to characterize the BNS within the crust. We find a region of low seismic velocity extending to about 30 km depth, located near 32°N. A minimum-structure magnetotelluric model [*Wei et al.*, 2001] shows little signature associated with the BNS, whereas more finely parameterized models [*Solon et al.*, 2000; *Solon*, 2000] allow complex near-surface resistivity and a low-resistivity body located near the BNS in the middle and lower crust. A change in lithology or the presence of a fractured/sheared zone could explain the low velocities at the BNS. Fluid accumulations in a fractured zone would be consistent with low resistivity values.

[18] Aeromagnetic data across the BNS [*Liu*, 1989] show distinct anomalies corresponding with known outcrops of serpentinized peridotite but are otherwise generally smooth (Figure 6; see locations of ophiolite in Figure 1). This magnetic pattern suggests that either peridotite at depth is not serpentinized (unlikely, given that peridotite at the surface is highly serpentinized) or that no major ophiolite is present in the subsurface. This observation is in contrast to the Yarlung-Zangbo Suture where a pronounced aeromagnetic anomaly is linked to the large bodies of ultramafic ophiolite believed to exist at depth [*Makovsky et al.*, 1999]and mapped at the surface [*Liu et al.*, 1986]. Better known examples elsewhere in the world include the Great Valley of California where a 10-km-thick ophiolite in the midcrust gives rise to a clear magnetic signature associated with the presence of the large ophiolite at depth rather than individual anomalies associated with bodies of serpentinite at the surface [*Cady*, 1975; *Godfrey and Klemperer*, 1998].

[19] On the basis of geologic evidence, *Girardeau et al.* [1986] and *Yin et al.* [1988] hypothesize that the oceanic crust corresponding with the ophiolite masses of the BNS was formed above a subduction zone during the Late Triassic to mid-Jurassic (Figure 2b). That the suture zone includes only a minimal volcanic arc (evidenced by scattered small granite bodies, and little or no arc volcanic rock) suggests that the closure of this basin may have included only minimal subduction. INDEPTH III seismic data show no evidence for high-velocity subducted oceanic crust beneath or within the Qiangtang block. In addition, evidence for anomalously warm mantle material beneath the Qiangtang block [*McNamara et al.*, 1997; *Wittlinger et al.*, 1996] is not consistent with the presence of cold slab material that would be associated with a long-lasting subduction environment. Though the signature of a subducted slab could have been obscured by magma injection, the lack of this signature is at least consistent with the other evidence mentioned. Thus we conclude that the ophiolite associated with the BNS was formed in a narrow basin (forearc or back arc) that existed between the Lhasa and Qiangtang blocks during the early Mesozoic (perhaps created by the subduction of Songpan-Ganzi to the north) and that little subduction was associated with the closure of this basin (Figure 2c).

[20] A tempting explanation for why the ophiolitic fragments are located as much as 150 km south of the suture zone is that they were emplaced by lateral motion along the several prominent strike-slip faults located near the main outcrops of ophiolite at Xainxa and Gyanco/Donqiao. However, the few tens of kilometers of displacement estimated along these faults by *Armijo et al.* [1989] is insufficient to account for the long distance spanned by the ophiolitic fragments to the south of the BNS. Another possible explanation is that the southern ophiolite bodies are indicative of another suture within the Lhasa block [e.g., *Matte et al.*, 1996], but little supporting evidence exists for such a feature.

[21] The shallow extent of the signature of the BNS suggests that the BNS is unrelated to the upward step in the Moho and the changes in upper mantle properties that occur beneath the suture. If the two features were related, we might expect to find that the low seismic velocities associated with the shallow suture would extend to the Moho, or that seismic reflections from such a structure would be present in our reflection data. Low seismic velocities in the crust of northern Tibet [*Zhao et al.*, 2001] indicate low density material there. Low Pn velocities and high attenuation of Sn phases beneath the northern Tibetan Plateau suggest an anomalously warm upper mantle. The thinner crust in the north and the laterally continuous elevation of the plateau can be explained by lower density crust in the north or support there by warm and less-dense mantle.

[22] In order to explore the issue of plateau isostatic support, we used velocity-density regression parameters [*Christensen and Mooney*, 1995, Table 8] to calculate lithostatic density columns for the Lhasa and Qiangtang blocks (Figure 7) from our velocity model (Figure 4) [*Zhao et al.*, 2001]. For the mantle lithosphere beneath the Qiangtang block we use a density of 3320 kg/m^3 [*Ringwood*, 1975]. The density for the uppermost 5 km of crust is taken to be the average of reasonable end members as determined for each block. For the Lhasa block, the lower plausible bound is ρ = 2440 kg/m^3 (1 km unconsolidated sediments over 4 km sedimentary rock using velocity-

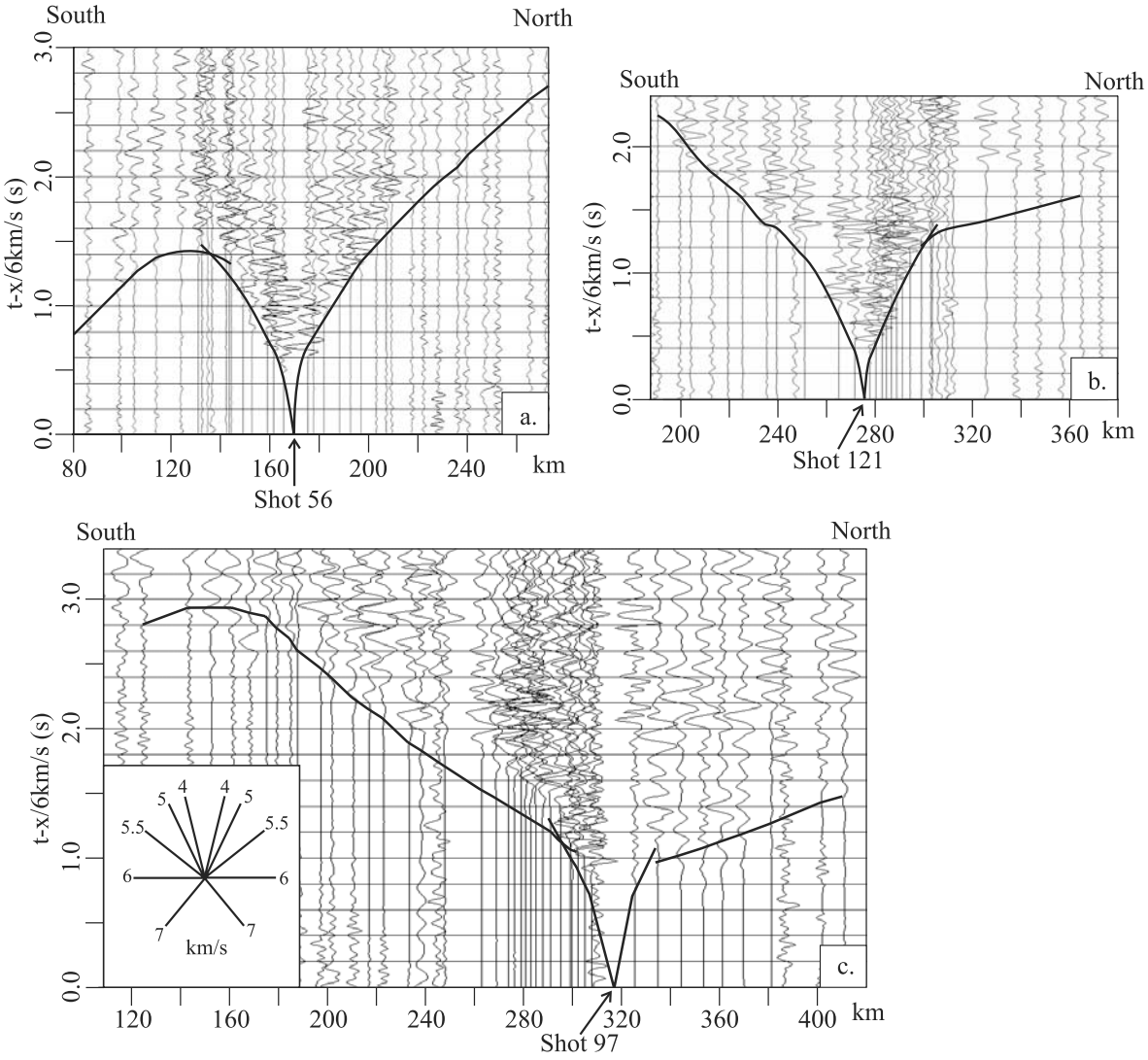

Figure 5. Shot gathers from three shots distributed along the INDEPTH III transect, overlain by arrivals predicted by the velocity model (Figure 4b). Reduction velocity 6 km/s; horizontal scale refers to positions along velocity model (Figure 4c). Amplitudes scaled using automatic gain control. a) Shot gather from shot 56 (50 kg shot, just south of BNS). Note high-velocity first arrivals on southern offsets corresponding with the Bangoin granite (>6 km/s), and low-velocity arrivals corresponding with the BNS. b) Shot gather from shot 121 (50 kg shot, south of Shuang Hu). Note low-velocity first arrivals corresponding with the thick sedimentary sequences on the southern Qiangtang block, and the sharp transition to a high-velocity (5.8 km/s) unit in the northern Qiangtang block. c) Shot gather from shot 97 (1 ton shot, near Shuang Hu). Note low-velocity first arrivals corresponding with the thick sedimentary sequences on the southern Qiangtang block, and the sharp transition to a high-velocity (5.8 km/s) unit in the northern Qiangtang block. Discrepancy of fit between northern receivers of shots 121 (model prediction precedes arrival) and 97 (model prediction lags arrival) is a result of fitting a two-dimensional model to a three-dimensional data set.

density relations after *Gardner et al.* [1974]) and the upper bound is $\rho = 2700$ kg/m^3 (granite extending to the surface). For the Qiangtang block, the lower bound is $\rho = 2430$ kg/m^3 (0.5 km of unconsolidated sediments above 4.5 km of sedimentary rock) and the upper bound is $\rho = 2550$ kg/m^3 (sedimentary units extending to the surface). Lateral density variations for the upper 5 km can change the total calculated pressure by up to 10 MPa. Densities corresponding to the velocity model of *Zhao et al.* [2001] indicate that crustal density differences alone can maintain isostatic balance despite the flat plateau topography and northward crustal thinning of Tibet because the Qiangtang velocity function is so much slower than the Lhasa block velocity function, particularly in the upper crust. The total pressure beneath

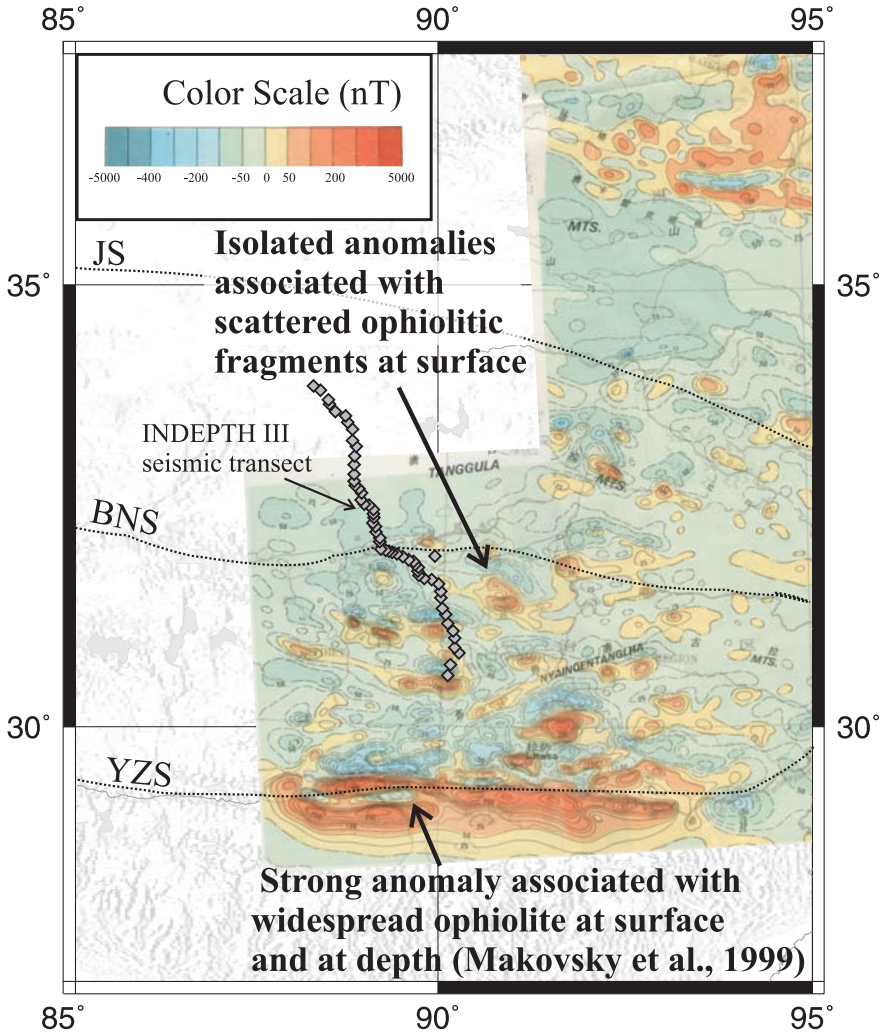

Figure 6. Aeromagnetic data [*Liu*, 1989] for eastern Tibetan Plateau. Data are not available for western plateau. Note pronounced anomaly associated with YZS and lack of anomaly associated with BNS. Scale of map is same as Figure 1.

the Lhasa block at the Moho (65 km) is 1.829 GPa, whereas the pressure beneath the Qiangtang at 65 km is found to be 1.832 Gpa, a difference of only 0.003 GPa (0.03 kbar) (Figure 7). Thus the northward step-up of the Moho near the BNS, with no accompanying elevation change, does not imply a change in mantle density and should not be used as corroborating evidence for the variations in mantle density argued for from teleseismic results [e.g., *Wittlinger et al.*, 1996; *McNamara et al.*, 1997; *Huang et al.*, 2000]. Previous gravity studies lacking our constraints on density (via velocity) and crustal thickness have assumed constant crustal density and either changes in mantle density [*Jin et al.*, 1996], or crustal thickness variations not supported by our data [*Braitenberg et al.*, 2000] to explain the Tibetan gravity field. Our result also provides a reasonable explanation for the change in Moho depth that occurs beneath the surface trace of the BNS without indicating that the trace of the BNS extends to the Moho. In fact, the change in depth to Moho is explained mainly as a result of upper crustal density variations, rather than as a product of any sort of variations in the lower crust beneath the BNS.

[23] The underthrusting of southern Tibet by Indian lithosphere north to about 32°N (coincidentally close to the surface location of the BNS, at the present time) remains the best explanation for the change of physical properties of Tibetan lithosphere at that latitude [*Owens and Zandt*, 1997]. The dearth of any sort of signature of the BNS vertically (or sub-vertically) in the lower crust beneath its surface location may indicate that this feature (assuming that it once existed) has been eradicated by lower crustal processes. Thus, we advocate models for plateau development that involve large-scale motion of middle and lower crustal material beneath the suture.

3.2. Qiangtang Block

[24] The deepest-seated rocks exposed in the Qiangtang block are early Mesozoic blueschist-bearing metamorphic

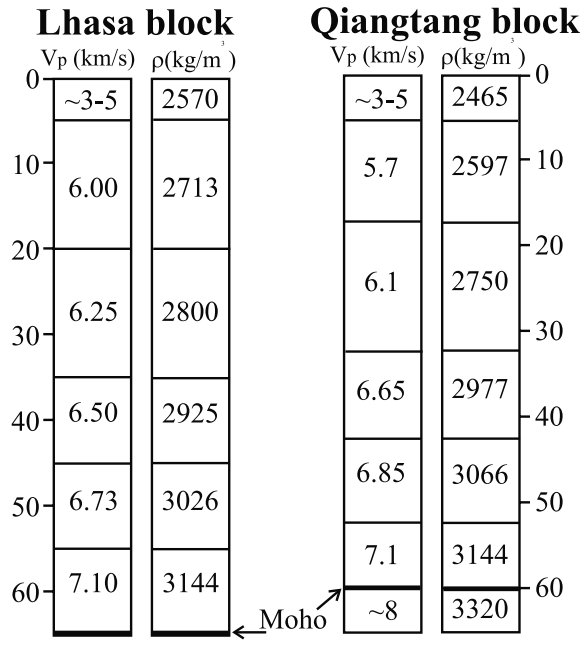

Figure 7. Velocity (V_p) and density (ρ) columns for the Lhasa and Qiangtang blocks. Total pressure beneath the Lhasa and Qiangtang blocks at 65 km depth is the same to within 3MPa (0.03 kbar), indicating that isostatic compensation is achieved within the crust. Density was calculated using the velocity-density regression parameters of *Christensen and Mooney* [1995, Table 8]. Crustal velocities are from *Zhao et al.* [2001], averaged over the swaths shown in Figure 4. Total pressure is calculated by summing the product ρgh for each column, where g is gravitational acceleration (9.8 m/s^2), considered to be constant within the columns, and h is the thickness of each layer within the column. Layers in velocity and density columns were designed to best represent the velocity gradients within each layer of the Vp model of *Zhao et al.* [2001].

units exhumed by Late Triassic-Early Jurassic low-angle normal faults. Exposures of these units form an E-W trending metamorphic belt interpreted to represent a large volume of melange emplaced during the southward subduction of Songpan-Ganzi oceanic lithosphere beneath the Qiangtang block in the early Mesozoic (Figure 2b) [*Kapp et al.*, 2000]. Field measurements at a melange outcrop near Shuang Hu, ~10 km east of the INDEPTH III seismic array, show the bounding Falong Detachment dipping steeply at the surface [*Kapp et al.*, 2000] (Figure 8).

[25] The arrival of a distinct seismic phase at receivers in the northernmost part of the INDEPTH III seismic array from shots north and south of Shuang Hu indicates a transition from a velocity of <5 km/s to a velocity of 5.8 km/s at a depth of about 3 km (see Figures 4b, 5b, and 5c). In the vicinity of Shuang Hu, the INDEPTH III seismometers are located within a half graben down-dropped ~6–8 km along the 13.5 Ma Shuang Hu normal fault (Figure 8a) [*Blisniuk et al.*, 2001; *Yin et al.*, 1999]. However, because of the crooked-line geometry of the INDEPTH III seismic array and because of the low-velocity material within the graben, most of the material sampled by ray paths in the Shuang Hu area from shots north and south of the map area (Figure 8a) lies to the west of the Shuang Hu normal fault. Thus the depth to the Falong Detachment or other geologic features indicated by the results presented here is the depth to those features on the footwall side of the Shuang Hu normal fault and inferences regarding offset on that normal fault can not easily be drawn from our data.

[26] Our preferred interpretation (Figure 8b) is that the velocity contrast corresponds with the contact between Triassic strata and the metamorphic core complex. This interpretation therefore suggests that the Falong Detachment flattens at a shallow depth [cf. *Kapp et al.*, 2000], so that the melange remains at shallow depths to the north of the core complex exposure. Alternatively (Figure 8c), the velocity increase could represent a contact between Triassic and Paleozoic units within the Qiangtang crust, above the Falong Detachment (at unknown depth), and the melange would represent a smaller component of the crust. Although high-seismic-velocity limestone exists within the Triassic strata [*Yin et al.*, 1999], we doubt that these units cause the observed velocity contrast because low-velocity shales continue beneath the thin limestone units.

[27] In our preferred model, the melange must be of regional extent beneath the northern plateau (Figure 9a), consistent with the conclusions of *Yin and Harrison* [2000] and consistent with our observations of the relatively low seismic velocity of the Qiangtang crust. Hence our model for plateau development must account for the underthrusting of a large volume of Songpan-Ganzi material beneath the Qiangtang block in order to emplace the melange. The original Qiangtang lower crustal material in a later section has been displaced, presumably by lower crustal flow (see below).

3.3. Crustal Fluids in Northern Tibet

[28] The combined data sets of INDEPTH III active- and passive-source seismic and magnetotelluric surveys reveal less evidence for fluid concentrations along the main INDEPTH III seismic transect in central Tibet (Figure 9a) than do data from southern and eastern Tibet. Minimum regional electrical resistivity values for the main INDEPTH III transect (~20 Ωm) presented by *Wei et al.* [2001] are much higher than those found in southern Tibet (~3 Ωm) [*Chen et al.*, 1996]. The more highly parameterized inversion of *Solon* [2000] shows low electrical resistivity values (~4 Ωm) locally beneath the BNS, possibly indicating the presence of fluids within the suture zone. Surface-wave analysis along the same transect shows no crustal low-velocity zone [*Rapine et al.*, 2002], a result supported by velocity modeling of active-source seismic data [*Zhao et al.*, 2001] and by the lack of pronounced high-amplitude reflections (bright spots) in reflection profiles. In contrast,

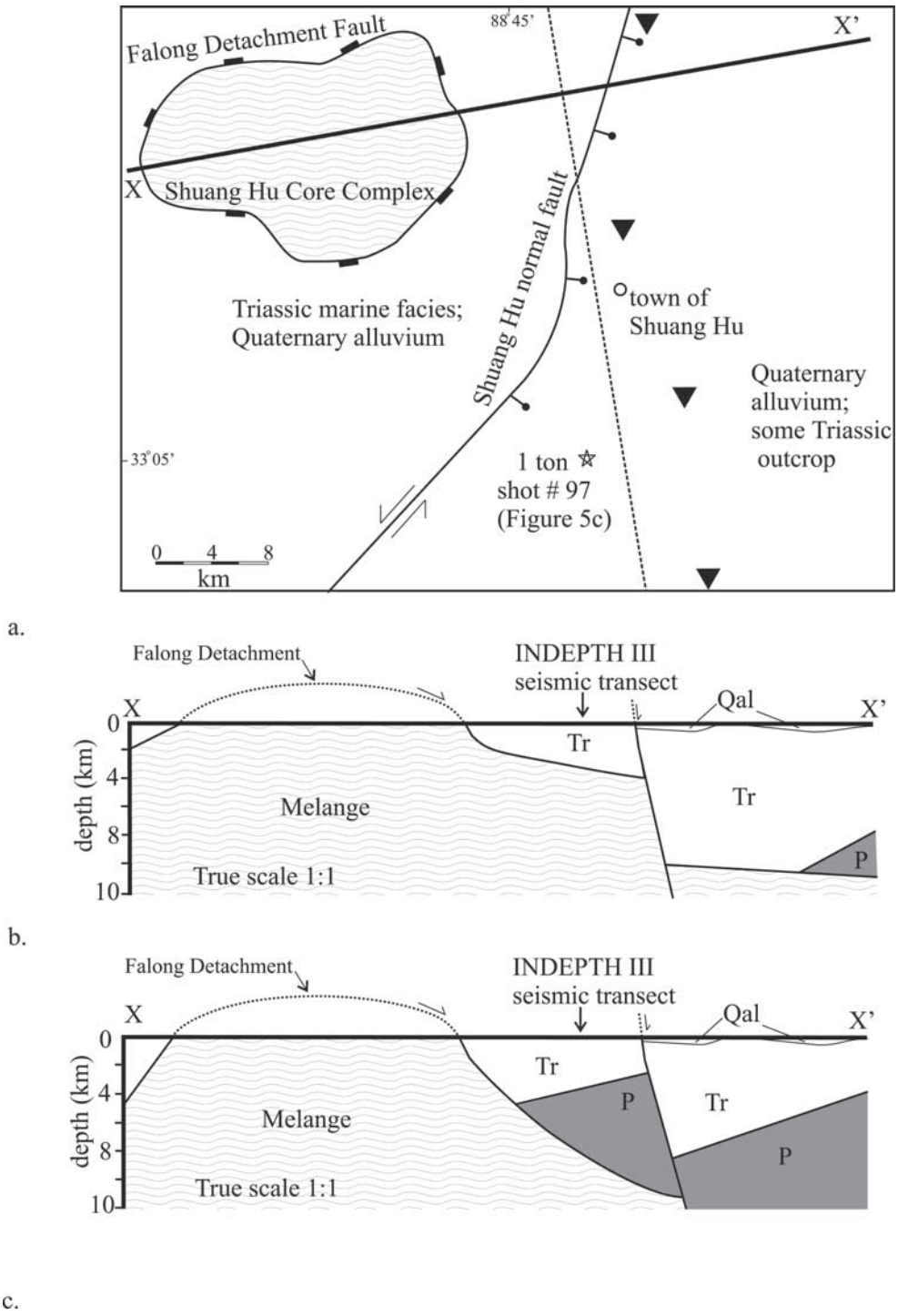

Figure 8. Detail of Shuang Hu area, after *Kapp et al.* [2000] and *Yin et al.* [1999]. a) map showing melange core complex, Shuang Hu normal fault, location of shot 97 (data in Figure 5c), black triangles marking locations of INDEPTH seismometers, dashed line showing 2-D approximation of INDEPTH III seismic transect; b) possible E-W cross section with Falong Detachment as the ~3-km-deep interface required by seismic data; c) possible E-W cross section with base of Triassic strata as the ~3-km-deep interface. Tr: Triassic, P: Paleozoic.

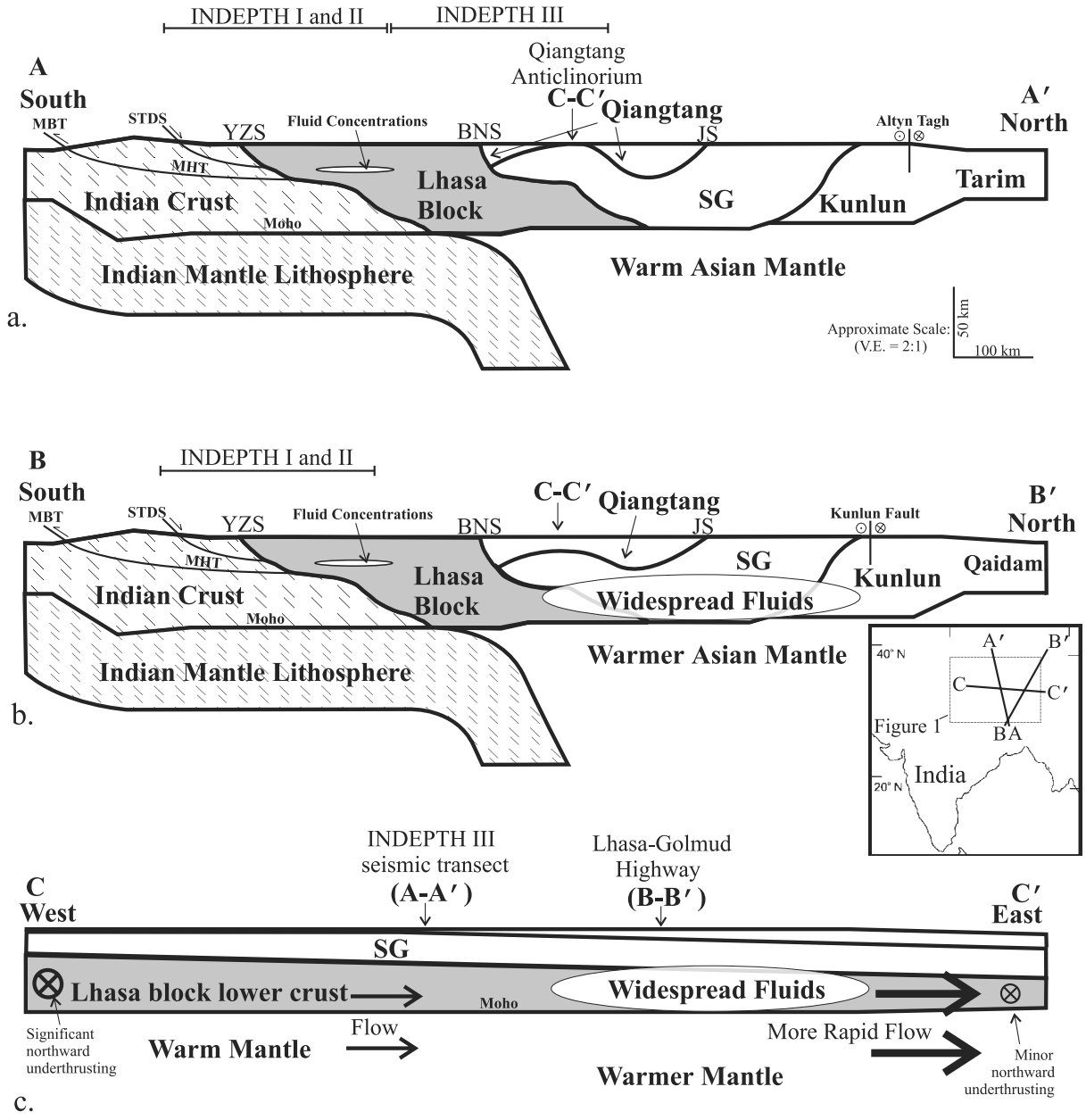

Figure 9. Generalized cross sections of the Tibetan Plateau along transects shown in inset and Figure 1: a) A-A′, SSE–NNW in central Tibet, along the INDEPTH III seismic transect, b) B-B′, SSW-NNE in eastern Tibet, along the Lhasa Golmud Highway, c) C-C′, W-E across the central Qiangtang block. Songpan-Ganzi Terrane (SG), South Tibetan Detachment System (STDS), Main Boundary Thrust (MBT), Main Himalayan Thrust (MHT) and other abbreviations as in Figures 1 and 2 [after *Nelson et al.*, 1996; *Yin and Harrison*, 2000; *Owens and Zandt*, 1997].

magnetotelluric studies in northeastern Tibet along the Lhasa-Golmud highway (Figure 9b), detect highly conductive (∼3 Ωm) crust consistent with fluid accumulations more extensive even than those in southern Tibet [*Wei et al.*, 2001]. Unfortunately, active-source seismic data have not been collected along the Lhasa-Golmud highway for comparison with the magnetotelluric data.

[29] The lack of bright spots in INDEPTH III seismic reflection data (CMP profiles and wide-angle data) suggests, but does not require, the absence of fluid concentrations in the central Tibet survey area. For comparison, individual bright spots imaged in southern Tibet span an in-line distance of as much as 25 km, though much of this apparent length may be due to diffraction from multiple smaller concentrations (1 to 2 km) [*Makovsky and Klemperer*, 1999]. The resolution of these concentrations was made possible by the collection of common midpoint data along ∼200 km of the 300-km INDEPTH II transect. Along

the 400-km INDEPTH III transect, true common midpoint profiling (with 16 m midpoint spacing—Geometrics data) was limited by cost to only about 17 km length, though augmented by about 60 km of profiling with ~125-m midpoint spacing (RefTek data). Thus the INDEPTH III data indicate only that fluid concentrations are not present on the 20% of the INDEPTH III transect that is well sampled (including much of the northern 80 km of the Lhasa block).

[30] On the basis of consideration of all the available evidence, we conclude that fluid bodies are not widespread along the main INDEPTH III seismic transect. The available data are consistent with either diffuse crustal fluids or a dry but hot crust for the INDEPTH III seismic transect [cf. *Hacker et al.*, 2000]. We conclude that melt north of 31°N is most prevalent in eastern Tibet (along, and east of, the Lhasa-Golmud highway; Figures 1 and 9b), and may be related to the proposed flow of lower crustal [*Clark and Royden*, 2000] or upper mantle [*Huang et al.*, 2000] material to the east. These fluids may be a result of shear heating caused by ductile flow [e.g., *Huang et al.*, 2000]; or they may be a result of heating from a mantle diapir [*Wittlinger et al.*, 1996], and a facilitator of ductile flow. A west-east variation in physical properties (Figure 9c) of the lithosphere is suggested by several different data sets. Magnetotelluric results from northern Tibet (previously described) and new results from southern Tibet [*Unsworth et al.*, 2001] show that higher conductivity values (and likely also correspondingly greater amounts of crustal fluids) exist in the crust of eastern Tibet than western Tibet, at least to the northern end of the INDEPTH III seismic transect (~200 km north of the BNS). That the zone of high Sn attenuation under northern Tibet (shown on Figure 1) extends eastward beyond the plateau margin but extends westward only to a distance of several hundred kilometers from the western plateau margin [*McNamara et al.*, 1995] is also consistent with a relatively greater percentage of crustal fluids under eastern regions of the Tibetan Plateau. Thus we must take into account this apparent west-east gradient as we consider models for plateau uplift and evolution.

3.4. Crustal Thickening Mechanisms

[31] A comparison between velocity models for the Tibetan crust and the global-average crustal velocity models [*Christensen and Mooney*, 1995] (Figures 3a and 10a) shows that the most fundamental difference between the global average and the velocity functions from Tibet is crustal thickness. We consider the Tibetan crust north of the Himalaya to be an average of 65 km thick [e.g., *Zhao et al.*, 2001], approximately 1.5 times the thickness of average continental crust. We apply the six crustal-thickening mechanisms of Figure 3 to the average velocity-depth function of *Christensen and Mooney* [1995] to increase the thickness to 65 km. We ignore the increase in velocity due to higher pressure, and the decrease in velocity due to higher temperature, because the effects tend to cancel such that the net changes are small (approximately +0.01 km/s for granite moved from 5 km to 30 km depth, and approximately −0.10 km/s for mafic granulite moved from 30 km to 50 km depth [*Christensen and Mooney*, 1995]).

[32] The thickening mechanisms tested represent the range of models proposed for the plateau, and give an estimate of the velocity structure that would be expected for each. They are not intended to stand individually as realistic models of plateau development, but rather to illustrate the velocity trends that would result from each mechanism. Wholesale crustal underthrusting (Figures 3b and 10b) would result in high-velocity lower crustal material at midcrustal depths, a pattern not seen in the velocity functions from Tibet. Injection models [e.g., *Zhao and Morgan*, 1987] predict normal thickness upper crust above pure shear thickened middle and lower crust, again requiring upper crustal velocities considerably higher than those found in Tibet (Figures 3c and 10b). In addition, these models imply the loss of Indian upper crustal material, a mechanism unsupported by geologic evidence.

[33] The fit of the global average velocity function to our measured Tibetan velocities (arithmetically averaged over ~50-km swaths of the Vp model of *Zhao et al.* [2001], shown in Figure 4c) is best when lower crust is lost from the system, as when the average crust is thickened by a pure-shear mechanism accompanied by removal of lower crust either via ductile flow or eclogitization (Figures 3e, 3g, and 10b). Fit is also reasonable for pure-shear thickening with (Figure 3f) or without (Figure 3d) lateral ductile flow of only the midcrust. In general, Tibetan crust shows somewhat greater proportions of upper (sialic) crust relative to lower (mafic-granulitic) crust when compared to the global average. Because the Qiangtang block upper crustal velocities are low to a great depth (~30 km), it is unlikely that this crust is a result of tectonic alteration of previously average crust. The present velocity structure requires a lithologic difference from average crust, perhaps related to the large volume of melange material believed to make up much of the crust of northern Tibet [*Yin and Harrison*, 2000].

[34] Additional constraint can be placed on uplift mechanisms by the amount of convergence that has occurred between India and Asia since the ~50 Ma collision. *Yin and Harrison* [2000] use geological observations to estimate convergence of >1400 km, though 360 km of this convergence was accommodated in the Nan Shan, north of the plateau itself. Seafloor spreading indicates convergence of ~1800 km in western Tibet and ~2750 km in eastern Tibet [*Dewey et al.*, 1989], though a portion of this convergence was likely accommodated north of the plateau. On the basis of an average north-south 1000-km width of the Tibetan Plateau, convergence of 1 to 1.5 times the width of the plateau must be explained. 150% pure-shear thickening of average crust (corresponding with 50% convergence) can produce 65-km-thick Tibetan crust, but any convergence >50% of the original width of the crust (~500 km of convergence) necessitates removal of material in order to produce crust that is only 65 km thick. Even if the convergence was accommodated by underthrusting/thickening of blocks with rifted margins and an average thickness of only 32.5 km, convergence in excess of 1000 km still necessitates removal of material in order to leave crust that

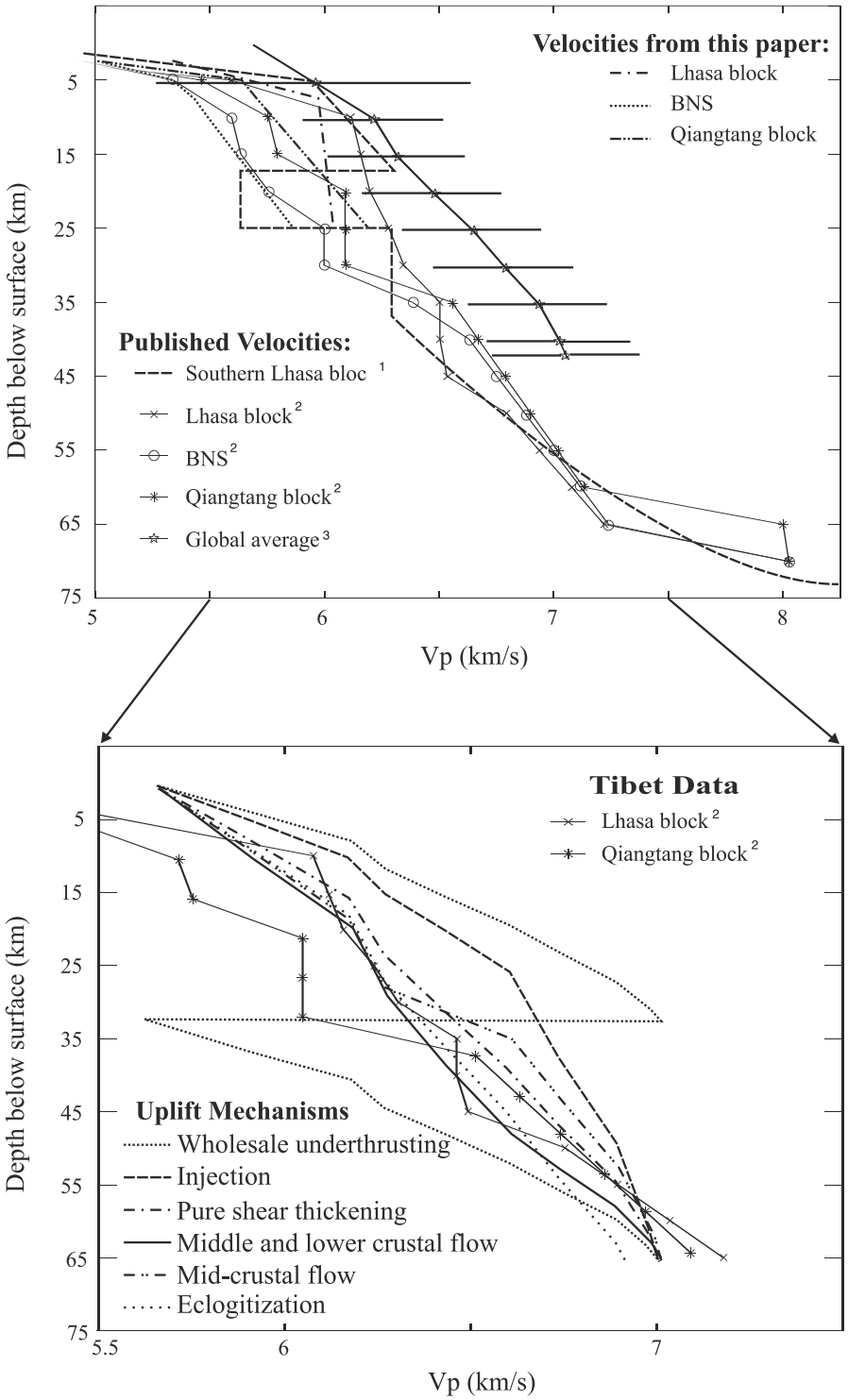

Figure 10. *P* wave velocity versus depth plots, a) showing velocity functions averaged over three areas (Lhasa Block, BNS, Qiangtang Block) from shallow velocity model of this paper plotted with published velocity-depth functions from [1]*Kola-Ojo and Meissner* [2001], [2]crustal-scale model of *Zhao et al.* [2001], and [3]global average of *Christensen and Mooney* [1995]; b) global-average velocity function thickened to represent 65-km-thick crust through each of six different mechanisms, with velocity functions from Lhasa and Qiangtang blocks for comparison (Qiangtang block velocity-depth function has been smoothly stretched to 65 km for ease of comparison).

is only 65 km thick. Pure-shear doubling of normal thickness crust accompanied by loss of ~50% of the initial volume of the lower half of the crust (see Figures 3e and 3g) can also accommodate only 100% convergence (1000 km). In order to achieve 1500 km of convergence while fitting our velocity profiles for the plateau, we must underthrust/thicken previously thinned crust and remove ~50% of the lower crust. The loss of lower crust may occur partially as conversion from seismic crust to seismic mantle by eclogitization (Figure 3g) but is probably mostly due to lateral escape by ductile flow (Figures 3e, 3f, and 9c). We favor ductile flow over eclogitization because the presence of large quantities of eclogite in the upper mantle (a thickness of 15 to 20 km corresponds with loss of ~50% of the lower crust) would inhibit plateau uplift and would be evidenced by high seismic velocities not compatible with the slow velocities and poor signal propagation found beneath northern Tibet. In addition, thermal models [*Henry et al.*, 1997] suggest that while eclogitization may be common beneath some mountain belts, it is unlikely beneath the Himalayas due to cold underthrust material and fast convergence rates. The loss of crustal material via large-scale lateral motion along strike-slip faults [e.g., *Molnar and Tapponier*, 1975] can accommodate greater convergence, or can permit the original crust to have been of average 42-km thickness or even to have been tectonically thickened [e.g., *Murphy et al.*, 1997] to >42 km prior to the India-Asia collision.

[35] While erosion has locally removed a great thickness of material near the plateau margins (e.g., 25 km in the southern Himalaya and 4 km in the Gangdese arc as discussed by *Fielding* [1996]), the interior of the plateau has lost little material through erosion. Thus, as a percentage of the total plateau volume, the material removed by erosion is small and does not enter our discussion in a quantitative sense. Inclusion of erosion would permit our models to accommodate greater convergence or initially thicker crust, or to include a smaller volume of material lost via ductile flow.

3.5. Crustal Evolution in Tibet

[36] We propose that the Qiangtang and Lhasa blocks were originally parts of a single block (Figure 2a) with lower-than-average-velocity upper crust and average-velocity lower crust. During the early Mesozoic, a large quantity of Songpan-Ganzi material was subducted beneath the northern margin of what became the Qiantang block, and the Lhasa block rifted from the Qiangtang block (Figure 2b). The resulting rift closed during the Late Jurassic to Early Cretaceous with the formation of the BNS (Figure 2c). The Lhasa block was thickened by pure shear beginning in the Cretaceous, and was intruded by large bodies of granite in the Cretaceous and Tertiary (e.g., the Gangdese batholith and Bangoin granite) that increased the average velocity of the upper crust (Figure 2d). Lhasa-block lower crustal material was thrust beneath the Qiangtang block [*Yin and Harrison*, 2000], as the Lhasa block was underthrust by Indian lower crustal material (see Figures 2f, 9a, and 9b). This chronology fits well with the BNS-reactivation scenario that *Roger et al.* [2000] propose in their interpretation of the Eocene magmatic belt that they identify across central Tibet. In order to achieve its current velocity structure, the Qiangtang block must have lost a large amount of lower crust relative to upper crust (assuming that lower crustal material was originally present) in order to accommodate underthrusting by Lhasa-block lower crust from the south and underthrusting by Songpan-Ganzi crust from the north (Figures 2f, 9a, and 9b). The loss of a lesser quantity of Lhasa-block lower crustal material is also suggested by the velocity structure as described above.

[37] Ductile lateral flow (Figure 9) [e.g., *Clark and Royden*, 2000] provides a reasonable and likely explanation for the loss of this lower crust, especially since the regionally smooth elevation of the plateau and results from gravity inversion suggest the presence of a ductile compensating layer at depth [*Fielding et al.*, 1994; *Jin et al.*, 1994]. In addition, shear-wave splitting results show a pronounced E-W fast direction in the Qiangtang block [*Huang et al.*, 2000; *McNamara et al.*, 1994; *Herquel et al.*, 1995], indicating strong E-W directed creep. Because the continental margin to the east is essentially a free edge (the Pacific subduction zones), it can be assumed that any flow would be to the east, an assumption supported by the gentle topographic slopes of the southeastern and northeastern plateau margins relative to the steep margins to the north, south, and west [e.g., *Clark and Royden*, 2000]. *Huang et al.* [2000] suggest that this flow takes place in the lower crust as well as in the upper mantle, on the basis of the spatially rapid transition from a null splitting result to large (up to 2.25 s) delay times at about 32°N. Lower crustal flow is also consistent with laminar reflectivity imaged at that depth by *Zhao et al.* [1999]. The extrusion of Tibetan lower crustal material to the east suggests that areas to the east of the Tibetan Plateau should be expected to show an abnormally great thickness of higher-velocity lower crustal material, a prediction that can easily be tested as new seismic data become available.

[38] An explanation for the low viscosity needed for ductile flow is provided by the fluid accumulations (likely melt) postulated to exist within the crust of eastern Tibet [e.g., *Wei et al.*, 2001] as described previously. The less viscous (likely warmer) material under eastern Tibet would facilitate channel flow (in a region where lateral extrusion is already more likely owing to its proximity to the eastern plateau margin), while the more rigid crust beneath central Tibet would be more conducive to underthrusting. Thus we propose an E-W gradient (Figure 9c), with lower viscosity and greater rapidity of channel flow in the east and greater rigidity and volume of underthrusting in the west.

[39] The underthrusting of Lhasa-block lower crustal material beneath the Qiangtang block in the Late Cretaceous–early Tertiary formed the Qiangtang Anticlinorium, one aspect of major ongoing regional compression [*Yin and Harrison*, 2000]. Then, facilitated by warmer (lower viscosity) material and the proximal free surface (eastern plateau margin), the lower crustal material beneath the eastern plateau began ductile flow to the east, driven by the plateau topography. Thinner lower crust beneath the eastern Qiangtang (relative to the western Qiangtang block)

provides an explanation for the eastward plunge of the Qiangtang Anticlinorium shown by *Yin and Harrison* [2000] (Figures 1 and 9). Our model for plateau development (Figures 2 and 9) combines the advantages of many previously proposed mechanisms, and agrees with available data. In particular, our model achieves the final velocity structure determined from INDEPTH III seismic data while incorporating the Indian plate underthrusting and lower crustal flow strongly suggested by various data sets.

4. Conclusions

[40] We have presented a new upper crustal *P* wave velocity model along a 400-km transect in central Tibet. Using this model, along with the whole-crustal velocity model presented by *Zhao et al.* [2001] and published aeromagnetic, geological, and other geophysical data, we conclude that:

1. The Bangong-Nujiang Suture has little geophysical manifestation and is the result of the closure of a forearc or back arc basin between the Lhasa and Qiangtang blocks, rather than being a full-fledged suture between two blocks that were once separated by a large ocean. We find no evidence that the Jurassic suture is related to changes in lower crustal and upper mantle properties with which it is fortuitously collocated along the INDEPTH III transect.

2. Velocity-depth functions suggest that the Lhasa and Qiangtang blocks were formed with slower-than-average seismic velocity upper crust, and average lower crust. Convergence was accommodated by a combination of pure-shear thickening and lower crustal underthrusting and removal of excess lower crustal material by lateral ductile flow (Figures 3e and 9).

3. The presence of crustal fluids in northern Tibet is limited to the eastern part of the plateau (the Lhasa-Golmud Highway, and farther east), and likely corresponds to the low viscosity required for ductile flow.

4. The plunge of the regional Qiangtang Anticlinorium can be explained as a result of eastward thinning of the underthrust Lhasa-block lower crustal material by ductile channel flow to the east.

5. The Qiangtang and Lhasa blocks are in approximate isostatic equilibrium at 65 km depth so that large mantle density differences to great depth below the BNS are precluded.

[41] **Acknowledgments.** We dedicate this paper to the memory of Doug Nelson (1953-2002), who was the intellectual leader of the INDEPTH group from its inception in 1992, as well as the field leader of three multi-disciplinary, multi-national field seasons on the Tibet plateau over the last decade. He was a good friend to all; we miss him. This manuscript has been greatly improved by the reviews of Craig Jones and Walter Mooney as well as thoughtful comments by Doug Nelson. We thank the 5th Geophysical Exploration Brigade of the Ministry of Land and Resources of China for providing logistical support under difficult circumstances in the field, along with the many Tibetans who helped to deploy our instruments. Essential financial support for the project was provided by the Ministry of Land and Resources, the National Natural Sciences Foundation of China, the U.S. National Science Foundation grant EAR-9614245-002, the Deutsche Forschungsgemeinschaft, and the GeoForschungsZentrum Potsdam (GFZ). An important phase of the data processing was conducted at GFZ, a trip made possible by support from the McGee Fund within the Stanford School of Earth Sciences. Klaus Bauer provided much needed assistance with the use of RayInvr. Some of the tectonic ideas presented here were developed through conversations with Paul Kapp. The field instruments were provided by the IRIS-PASSCAL and the GFZ Potsdam instrument pool; all seismic data are available from www.iris.edu. Generic Mapping Tools (GMT) was used to create Figures 1, 4, and 6.

References

Allegre, C. J., et al., Structure and evolution of the Himalaya-Tibet orogenic belt, *Nature*, *307*, 17–22, 1984.

Alsdorf, D., and K. D. Nelson, Tibetan satellite magnetic low: Evidence for widespread melt in the Tibetan crust?, *Geology*, *27*, 943–947, 1999.

Armijo, R., P. Tapponier, and T. Han, Late Cenozoic right-lateral strike-slip faulting in southern Tibet, *J. Geophys. Res.*, *94*, 2787–2838, 1989.

Barazangi, M., and J. Ni, Velocities and propagation characteristics of Pn and Sn beneath the Himalayan arc and Tibetan plateau: Possible evidence for underthrusting of Indian continental lithosphere beneath Tibet, *Geology*, *10*, 179–185, 1982.

Blisniuk, P., B. Hacker, J. Glodney, L. Ratschbacher, S. Bi, Z. Wu, M. McWilliams, and A. Calvert, Normal faulting in central Tibet since at least 13.5 Myr ago, *Nature*, *412*, 628–632, 2001.

Braitenberg, C., M. Zadro, J. Fang, Y. Wang, and H. Hsu, The gravity and isostatic Moho undulations in Qinghai-Tibet plateau, *J. Geodyn.*, *30*, 489–505, 2000.

Brown, L. D., W. Zhao, K. D. Nelson, M. Hauck, D. Alsdorf, A. Ross, M. Cogan, M. Clark, X. Liu, and J. Che, Bright spots, structure and magmatism in southern Tibet from INDEPTH seismic reflection profiling, *Science*, *274*, 1688–1690, 1996.

Cady, J., Magnetic and gravity anomalies in the Great Valley and Western Sierra Nevada metamorphic belt, California, *Spec. Pap. Geol. Soc. Am., 168*, 56 pp., 1975.

Chang, C., et al., Preliminary conclusions of the Royal Society and Academia Sinica 1985 geotraverse of Tibet, *Nature*, *323*, 501–507, 1986.

Chen, L., J. Booker, A. Jones, W. Nong, M. Unsworth, W. Wei, and H. Tan, Electromagnetic images of colliding continents: A magnetotelluric survey of the Tsangpo suture zone and surrounding regions, *Science*, *274*, 1694–1696, 1996.

Christensen, N., and W. Mooney, Seismic velocity structure and composition of the continental crust: A global view, *J. Geophys. Res.*, *100*, 9761–9788, 1995.

Clark, M., and L. Royden, Topographic ooze: Building the eastern margin of Tibet by lower crustal flow, *Geology*, *28*, 703–706, 2000.

Coward, M., W. Kidd, Y. Pan, R. Shackelton, and H. Zhang, The structure of the 1985 Tibet Geotraverse, Lhasa to Golmud, *Philos. Trans. R. Soc. London, Ser. A*, *327*, 307–336, 1988.

Dewey, J., S. Cande, and W. Pitman, Tectonic evolution of the Indian/Eurasian collision zone, *Eclogae Geol. Helv.*, *82*, 717–734, 1989.

Fielding, E., Tibet uplift and erosion, *Tectonophysics*, *260*, 55–84, 1996.

Fielding, E., B. Isacks, M. Barazangi, and C. Duncan, How flat is Tibet?, *Geology*, *22*, 163–167, 1994.

Gardner, G., L. Gardner, and A. Gregory, Formation velocity and density—The diagnostic basics for stratigraphic traps, *Geophysics*, *39*, 770–780, 1974.

Girardeau, J., J. Marcoux, C. Allegre, J. Bassoullet, Y. Tang, X. Xiao, Y. Zao, and X. Wang, Tectonic environment and geodynamic significance of the Neo-Cimmerian Dongqiao ophiolite Bangong-Nujiang suture zone, Tibet, *Nature*, *307*, 27–31, 1984.

Girardeau, J., J. Marcoux, E. Fourcade, J. Bassoullet, and Y. Tang, Xianxa ultramafic rocks, central Tibet China: Tectonic environment and geodynamic significance, *Geology*, *13*, 330–333, 1985.

Girardeau, J., J. Mercier, and Y. Tang, Petrology of the Donqiao-Xainxa ophiolite (North Tibet, China): Evidence for its formation in a supra-subduction zone environment, *Ofioliti*, *11*, 235–262, 1986.

Godfrey, N., and S. Klemperer, Ophiolitic basement to a forearc basin and implications for continental growth: The Coast Range/Great Valley ophiolite California, *Tectonics*, *17*, 558–570, 1998.

Hacker, B., E. Gnos, L. Ratschbacher, M. Grove, M. McWilliams, S. Sobolev, W. Jiang, and Z. Wu, Hot and dry deep crustal xenoliths from Tibet, *Science*, *287*, 2463–2466, 2000.

Henry, P., B. Goffe, and P. Henry, Kinematic, thermal and petrological model of the Himalayas: Constraints related to metamorphism within the underthrust Indian crust and topographic elevation, *Tectonophysics*, *273*, 31–56, 1997.

Herquel, G., G. Wittlinger, and J. Guilbert, Anisotropy and crustal thickness for northern Tibet: New constraints for tectonic modeling, *Geophys. Res. Lett.*, *22*, 925–928, 1995.

Hirn, A., A. Nercessian, M. Sapin, G. Jobert, Z. Xu, E. Gao, D. Lu, and J. Teng, Lhasa block and

bordering sutures—A continuation of a 500-km Moho traverse through Tibet, *Nature*, *307*, 25–27, 1984.

Houseman, G., and P. England, A lithospheric-thickening model for the Indo-Asian collision, in *The Tectonic Evolution of Asia*, edited by A. Yin and T. M. Harrison, pp. 3–17, Cambridge Univ. Press, New York, 1996.

Huang, W., J. Ni, F. Tilmann, K. D. Nelson, J. Guo, W. Zhao, J. Mechie, R. Kind, J. Saul, R. Rapine, and T. Hearn, Seismic polarization anisotropy beneath the central Tibetan Plateau, *J. Geophys. Res.*, *105*, 27,979–27,989, 2000.

Jin, Y., M. McNutt, and Y. Zhu, Evidence from gravity and topography data for folding of Tibet, *Nature*, *371*, 669–674, 1994.

Jin, Y., M. McNutt, and Y. Zhu, Mapping the descent of Indian and Eurasian plates beneath the Tibetan Plateau from gravity anomalies, *J. Geophys. Res.*, *101*, 11,275–11,290, 1996.

Kapp, P., A. Yin, C. Manning, M. Murphy, T. M. Harrison, M. Spurlin, L. Ding, X. Deng, and C. Wu, Blueshist-bearing metamorphic core complexes in the Qiangtang Block reveal deep crustal structure of Northern Tibet, *Geology*, *28*, 9–22, 2000.

Kidd, W., Y. Pan, C. Chang, M. Coward, J. Dewey, A. Gansser, P. Molnar, R. Shackelton, and Y. Sun, Geological mapping of the 1985 Chinese-British Tibetan (Xizang-Qinghai) Plateau Geotraverse route, *Philos. Trans. R. Soc. London, Ser. A*, *327*, 287–305, 1988.

Kola-Ojo, O., and R. Meissner, Southern Tibet: Its deep seismic structure and some tectonic implications, *J. Asian Earth Sci.*, *19*, 249–256, 2001.

Kosarev, G., R. Kind, S. Sobolev, X. Yuan, W. Hanka, and S. Oreshin, Seismic evidence for a detatched Indian lithospheric mantle beneath Tibet, *Science*, *283*, 1306–1309, 1999.

Liu, S., Aeromagnetic anomaly map of China and the adjacent sea areas (1:4000000), China Cartogr. Publ. House, Beijing, 1989.

Liu, Z., et al., Geological Map of Qinghai-Xizang (Tibet) Plateau and Adjacent Areas (1:1500000), Geol. Publ. House, Chengdu Inst. of Geol. and Miner. Resour., Chin. Acad. of Geol. Sci., Beijing, 1986.

Makovsky, Y., and S. Klemperer, Measuring the seismic properties of Tibetan bright spots: Evidence for free aqueous fluids in the Tibetan middle crust, *J. Geophys. Res.*, *104*, 10,795–10,825, 1999.

Makovsky, Y., S. Klemperer, L. Ratschbacher, and D. Alsdorf, Midcrustal reflector on INDEPTH wide-angle profiles: An ophiolitic slab beneath the India-Asia suture in southern Tibet?, *Tectonics*, *18*, 793–808, 1999.

Matte, P., P. Tapponnier, N. Arnaud, L. Bourjot, L. Avouac, P. Vidal, Q. Liu, Y. Pan, and Y. Wang, Tectonics of Western Tibet, between the Tarim and the Indus, *Earth Planet. Sci. Lett.*, *142*, 311–330, 1996.

McNamara, D., T. Owens, P. Silver, and F. Wu, Shear wave anisotropy beneath the Tibetan Plateau, *J. Geophys. Res.*, *99*, 13,655–13,665, 1994.

McNamara, D., T. Owens, and W. Walter, Observations of regional phase propagation across the Tibetan Plateau, *J. Geophys. Res.*, *100*, 22,215–22,229, 1995.

McNamara, D., W. Walter, T. Owens, and C. Ammon, Upper mantle velocity structure beneath the Tibetan Plateau from Pn travel time tomography, *J. Geophys. Res.*, *102*, 493–505, 1997.

Molnar, P., and P. Tapponier, Cenozoic tectonics of Asia: Effects of a continental collision, *Science*, *189*, 419–426, 1975.

Murphy, M., A. Yin, T. M. Harrison, S. Durr, Z. Chen, F. Ryerson, W. Kidd, X. Wang, and X. Zhou, Did the Indo-Asian collision alone create the Tibetan Plateau?, *Geology*, *25*, 719–722, 1997.

Nelson, K. D., et al., Partially molten crust beneath southern Tibet: Synthesis of project INDEPTH results, *Science*, *274*, 1684–1688, 1996.

Owens, T., and G. Zandt, Implications of crustal property variations for models of Tibetan Plateau evolution, *Nature*, *387*, 37–43, 1997.

Powell, C., and P. Conaghan, Plate tectonics and the Himalayas, *Earth Planet. Sci. Lett.*, *20*, 1–12, 1973.

Rapine, R., F. Tilmann, M. West, J. Ni, and A. Rodgers, Crustal structure of northern and southern Tibet from a surface wave dispersion analysis, *J. Geophys. Res.*, *107*, doi:10.1029/2001JB000445, in press, 2002.

Ringwood, A., *Composition and Petrology of the Earth's Mantle*, 618 pp., McGraw-Hill, New York, 1975.

Roger, F., P. Tapponnier, N. Arnaud, U. Schärer, M. Brunel, X. Zhiqin, and Y. Jingsui, An Eocene magmatic belt across central Tibet: Mantle subduction triggered by the Indian collision?, *Terra Nova*, *12*, 102–108, 2000.

Sapin, M., and A. Hirn, Seismic structure and evidence for eclogitization during the Himalayan convergence, *Tectonophysics*, *273*, 1–16, 1997.

Solon, K., Electromagnetic images of the Banggong-Nujiang Suture zone of central Tibet: From INDEPTH-III magnetotelluric data, M.S. thesis, 87 pp., Syracuse Univ., Syracuse, N. Y., 2000.

Solon, K., A. Jones, K. D. Nelson, M. Unsworth, W. Zhao, and W. Wei, Electromagnetic images of the Banggong-Nujiang suture zone of central Tibet: From INDEPTH III magnetotelluric data, *Eos Trans. AGU*, *81*(48), Fall Meet. Suppl., Abstract T52B-04, 2000.

Unsworth, M., et al., East-west variations in the crustal structure of the southern Tibetan Plateau from magnetotelluric data, *Eos Trans. AGU*, *82*(47), Fall Meet. Suppl., Abstract T12F-11, 2001.

Wei, W., et al., Detection of widespread fluids in the Tibetan crust by magnetotelluric studies, *Science*, *292*, 716–718, 2001.

Wittlinger, G., F. Masson, G. Poupinet, P. Tapponnier, M. Jiang, G. Herquel, J. Guilbert, U. Achauer, G. Xue, and D. Shi, Seismic tomography of northern Tibet and Kunlun: Evidence for crustal blocks and mantle velocity contrasts, *Earth Planet. Sci. Lett.*, *139*, 263–279, 1996.

Yin, A., and T. M. Harrison, Geologic evolution of the Himalayan-Tibetan orogen, *Annu. Rev. Earth Planet. Sci.*, *28*, 211–280, 2000.

Yin, A., P. Kapp, M. Murphy, C. Manning, T. M. Harrison, M. Grove, L. Ding, X. Deng, and C. Wu, Significant late Neogene east-west extension in northern Tibet, *Geology*, *27*, 787–790, 1999.

Yin, J., J. Xu, C. Liu, and H. Li, The Tibetan plateau: Regional stratigraphic context and previous work, *Philos. Trans. R. Soc. London, Ser. A*, *327*, 5–52, 1988.

Zelt, C., and R. Smith, Seismic traveltime inversion for 2-D crustal velocity structure, *Geophys. J. Int.*, *108*, 16–34, 1992.

Zhang, K., Blueshist-bearing metamorphic core complexes in the Qiangtang block reveal deep crustal structure of northern Tibet: Comment, *Geology*, *29*, 90, 2001.

Zhao, W., and W. J. Morgan, Injection of Indian crust into Tibetan lower crust: A two-dimensional finite element model study, *Tectonics*, *6*, 489–504, 1987.

Zhao, W., A. Ross, L. Brown, K. D. Nelson, S. Klemperer, S. Haines, J. Mechie, J. Saul, and J. Guo, Seismic bright spots and partial melting under the Tibetan Plateau, *Eos Trans. AGU*, *80*(46), Fall Meet. Suppl., F952, 1999.

Zhao, W., et al., Crustal structure of central Tibet as derived from project INDEPTH wide-angle seismic data, *Geophys. J. Int.*, *145*, 486–498, 2001.

Zhao, X., Y. Cao, M. Zhu, D. Xia, and D. Qian, Plate Tectonic-Lithofacies Map of Xizang (Tibet), China (1:1500000), Geol. Publ. House, Inst. of Geol. Sci., Bur. of Geol. and Miner. Resour. of Xizang (Tibet) Auton. Reg., Beijing, 1984.

L. Brown and G. Jingru, Department of Geological Sciences, Cornell University, Ithaca, NY 14853, USA.

S. S. Haines and L. Klemperer, Department of Geophysics, Stanford University, Stanford, CA 94305, USA. (shaines@geo.stanford.edu)

J. Mechie, GeoForschungsZentrum Potsdam (GFZ), Telegrafenberg A3, D-14473, Potsdam, Germany.

R. Meissner, Institute of Geophysics, Kiel University, D-24118 Kiel, Germany.

A. Ross, Geological Institute, University of Copenhagen, Oster Voldgade 10, Copenhagen, DK-1350 Denmark.

Z. Wenjin, Chinese Academy of Geological Sciences, Beijing, China.